JOURNAL OF SOLID STATE CHEMISTRY 50, 247–255 (1983)

Calcium Hydroxide Dehydration Early Precursor States

O. CHAIX-PLUCHERY AND J. BOUILLOT

Institut Laue-Langevin BP 156X, 38042 Grenoble Cedex, France

D. CIOSMAK AND J. C. NIEPCE

Laboratoire de Recherche sur la Réactivité des Solides, Faculté des Sciences Mirande, BP 138, 21004 Dijon Cedex, France

AND F. FREUND

Mineralogisches Institut Universität Köln, Zülpicher Strasse 49, 5000 Cologne 1, Federal Republic of Germany

Received April 4, 1983, and in revised form July 25, 1983

A neutron and X-ray diffraction study of coarsely polycrystalline $Ca(OD)_2$ shows that approximately 50°C below the onset temperature of dehydration, which is sensitive to the water partial pressure, slight structural modifications occur. They manifest themselves by a sudden sharpening of the 001 reflection and by a decrease in the slope of the 001 intensity vs temperature plots. The initially broad 001 reflections suggest that H_2O molecules first form statistically in the (001) planes by trapping protons on OH^- lattice sites, thus causing strains. At a critical temperature the H_2O molecules segregate into domain boundaries which are incapable of scattering neutrons coherently. At the same time the stresses in the domains are relaxed causing strain relaxation and the sharpening of the 001 reflexions. Dehydration is delayed until the domains coalesce and open fast diffusion pathways for the H_2O molecules.

Introduction

The present work is part of the studies related to the thermal decomposition mechanism of simple, primarily ionic, CdI_2-type hydroxides. Several steps are necessarily involved in the decomposition reaction.

Step (1): formation of H_2O molecules from OH^- ions;

Step (2): elimination of the H_2O molecules from the structure of the hydroxide;

Step (3): transformation of the hydroxide structure into the oxide structure.

Earlier studies of $Ca(OH)_2$ and $Cd(OH)_2$ (*1–4*) as well as $Mg(OH)_2$ (*5*) have indicated that step (2) involves the evaporation of the H_2O molecules from a transitory, high defect concentration relict structure. Step (3) comprises the transformation of this relict structure into the stable oxide structure. This transformation which occurs essentially at constant composition exhibits the morphological and structural features of a shear transformation (*1–4*).

Step (1), the formation of H_2O molecules in the yet intact hydroxide structure, has

0022-4596/83 $3.00

been studied by optical spectroscopy and proton conductivity (*6–8*). The results indicate that a small fraction of the hydroxyl protons becomes mobile, i.e., delocalized by thermal excitation to a proton conduction band. H_2O molecules are then formed when the mobile protons are trapped by OH^- ions. In the present work X-ray and neutron diffraction techniques were used to study the prereactional changes, step (1), occurring in $Ca(OH)_2$ and $Ca(OD)_2$ during heating, prior to the transformation into CaO.

Experimental

Samples. $Ca(OD)_2$ powder was prepared by precipitation from an aqueous solution, the reactants being NaOD and anhydrous $CaCl_2$ in D_2O. The preparation was done in a glove box in an H_2O- and CO_2-free atmosphere. $Ca(OD)_2$ crystallizes in the $P\bar{3}m1$ space group and the structure is given in Ref. (*9*). CaO has the NaCl structure.

Neutron diffraction. In a first experiment the D1B diffractometer was used equipped with a multidetection system composed of 400 counters spaced by 0.2° 2ϑ and covering a range from 24 to 104° 2ϑ. The wavelength was 2.522 Å. The first 5 $Ca(OD)_2$ diffraction lines were recorded with a counting time of about 1 hr for each diagram.

In a second experiment the D1A diffractometer was used equipped with a bank of 10 ^{3}He counters at an angular spacing of 6° 2ϑ. The wavelength was 1.909 Å. Using 0.05° increments the Bragg region was scanned up to 160° 2ϑ. Sixteen $Ca(OD)_2$ diffraction lines were thus recorded with a data acquisition time of about 10 hr for each diagram.

The vacuum chamber consisted of an Al cylinder with an internal heater made out of two Nb sheets and a thin-walled V cylinder, open at both ends, as a sample container (cross section: 1 cm, height: 10 cm). The $Ca(OD)_2$ powder was evenly dispersed on fused SiO_2 wool to assure an intimate contact with the experimental atmosphere.

X-ray diffraction. The setup used for the X-ray part of this study has been described earlier (*10, 11*). It consists of a ϑ, $-\vartheta$ horizontal axis goniometer equipped with a LETI linear detector (*12*), a multichannel analyzer and a monitoring screen. With Cu$K\alpha_1$ radiation, 1.54051 Å, selected by a bent quartz monochromator, each of the 1024 channels corresponds to an angular increment of 0.01734° 2ϑ. The detection window thus covered slightly more than 10° in 2ϑ.

Either a linear heating program (2.5 K-hr^{-1} for X-rays and D1B) or a stepwise temperature increment program (for D1A) were used. The experiments were carried out either in vacuum or under controlled water vapor pressures. The base pressure of 10^{-5} Torr was obtained with a liquid nitrogen cold trap near the sample chamber and was measured by a ionization gauge. In the experiments performed under controlled water vapor pressure, the sample chamber was connected to a fixed temperature water/ice reservoir after evacuation to 10^{-5} Torr.

For each recorded diffraction line, the integrated intensity and width were determined. For X-ray lines, the width is the integral breadth and in case of neutron lines the width is the full width at half maximum calculated after fitting the experimental profiles to Gaussian line shapes.

TABLE I

WIDTH w_h OF THE $Ca(OD)_2$ NEUTRON DIFFRACTION PEAKS AT 25°C AND INSTRUMENTAL WIDTH w_g OF THE D1B SPECTROMETER (FOR λ = 2.522 Å)

hkl	001	100	101	102	110
Θ(°Θ)	14.80	23.88	28.61	40.72	44.54
ω_g(°Θ)	0.175	0.205	0.240	0.400	0.455
ω_h(°Θ)	0.279	0.234	0.328	0.596	0.502

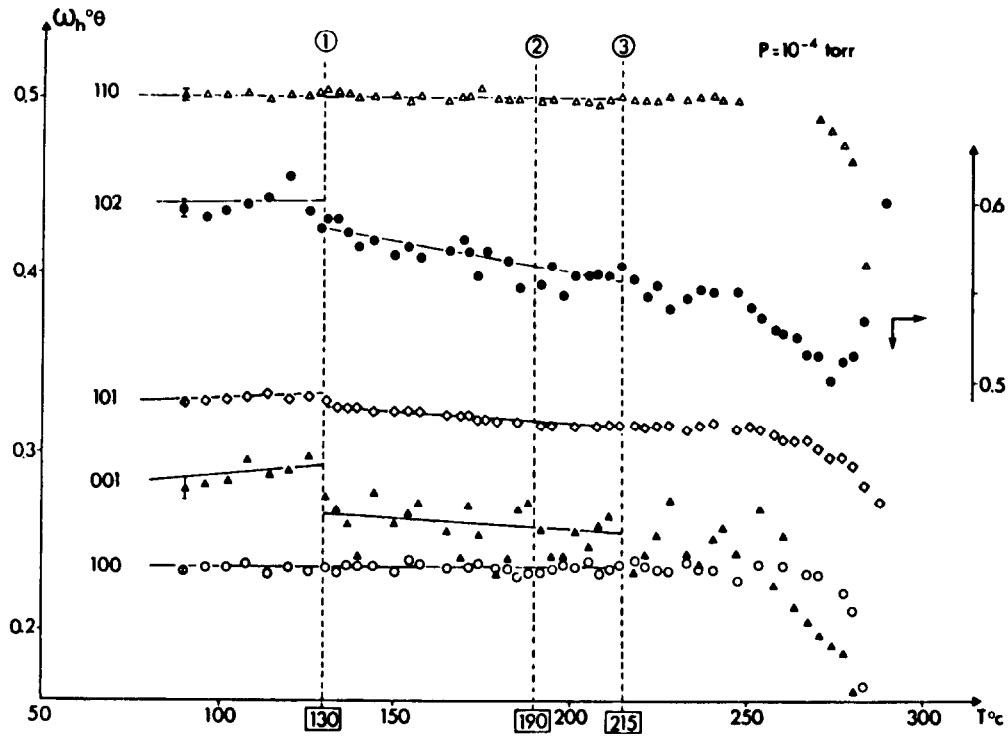

FIG. 1. Evolution of the width (in degrees ϑ) of the $Ca(OD)_2$ reflections as recorded as a function of temperature in vacuum by neutrons. The lines 1, 2, and 3 correspond to peak sharpening, first dehydration, and first appearance of CaO reflections, respectively.

Results

In Table I the experimental width values of the $Ca(OD)_2$ diffraction peaks at 25°C are compared with the instrumental width (resolution), of the D1B diffractometer. All reflections with $l \neq 0$ are considerably broadened, while the width of the reflections with $l = 0$ is close to the instrumental resolution.

Figures 1 and 2 show the temperature variation of the width of the reflections 001, 100, 101, 102, and 110, measured by neutron diffraction on the D1B, and of the reflections 102 and 110 measured by X-rays, in both cases in vacuum. All $hk0$ reflection widths remain constant up to the onset of the dehydration reaction which occurs around 190°C. All reflections with $l \neq 0$ exhibit a sudden sharpening around 130°C and, as is evident from Fig. 1, a continuous decrease of the width with further increase of temperature. This behavior is evidenced by the great number of observations, although the error bars are almost of the order of magnitude of the effect. The CaO diffraction peaks do not appear until >215°C.

The cause for the diffraction peak broadening may be either size effects or lattice strain. To differentiate between the two the Williamson–Hall analysis (*13*) was applied to harmonic families of the neutron diffraction peaks $00l$, $h0h$, and $h00$ obtained with the D1A. The results are shown in Fig. 3 where w_f is the peak broadening due to the sample only, i.e., corrected for the instrumental width w_g. The straight lines obtained can be written as $qx + r$ where q is propor-

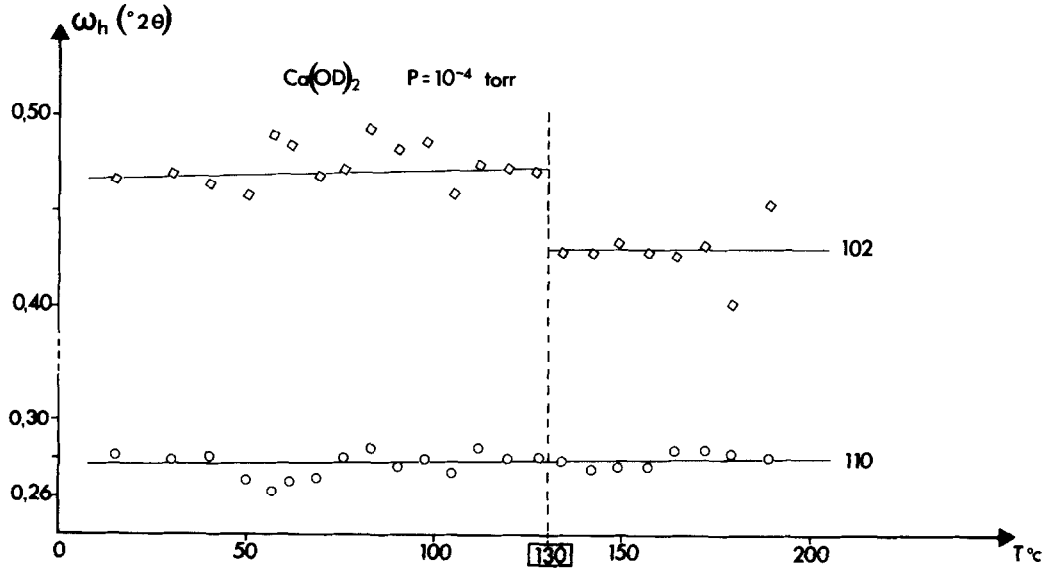

FIG. 2. As Fig. 1, recorded in vacuum by X-rays.

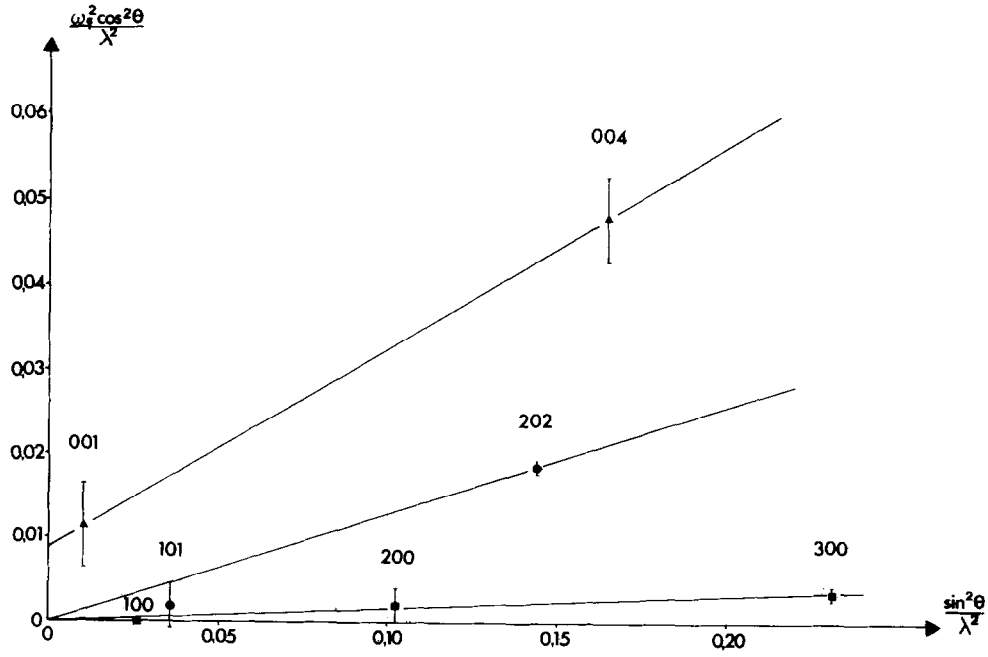

FIG. 3. Williamson–Hall plot of selected $Ca(OD)_2$ neutron diffraction peaks at 17°C (w_f is the linewidth corrected for instrumental broadening).

tional to the lattice strain and $1/r$ proportional to the square of the mean crystallite size normal to the planes considered.

The Williamson–Hall plot for the series 100, 200, 300 indicates that neutron beams coming in parallel to the basal (001) planes register large coherently scattering domains and a minimal lattice strain. As the incident neutron beam is turned towards the [001] direction (parallel to the threefold axis), the strain contribution increases due to lattice distortions in the (001) basal planes. In addition there will be stacking faults in the [001] direction affecting the intensity and width of the $00l$ reflections. This result is not unexpected because, being a layer structure, $Ca(OH)_2$ cannot sustain large strains except in the (001) basal planes. The nonzero r value for the series $00l$ suggests that a small crystallite size effect may exist in the [001] direction.

Figure 1 indicates that the strain in the (001) planes first increases with increasing temperature from ambient to 130°C and then decreases with increasing temperature above 130°C. The strain relaxation was found to be irreversible, i.e., the (001) strains remained low in the sample cooled from 200°C back to 108°C. It is to be noted, however, that the diffraction pattern at 108°C on which this latter statement is based was recorded only once immediately after cooling the sample from 200°C. If the strains returned slowly, the present data would not show it. We shall return to this point in the discussion section.

The same type of analysis can also be carried out on the X-ray diffraction profiles. After deconvolution using Stoke's method (*14*), the Fourier coefficients of the deconvoluted profile have been calculated. By applying the Warren–Averbach analysis (*15*) the behavior of the sample as shown by Fig. 3 is confirmed (*16*). Since the main contribution to the scattered X-ray intensity comes from the heavy atoms Ca, this implies that the atomic displacements due to strain and/or disorder are not confined to the D position only but affect lattice as a whole.

If the $Ca(OD)_2$ powder is heated under $P(H_2O) = 1.78$ Torr, the results obtained are essentially similar to those of the vacuum runs. Figures 4 and 5 show that the sharpening of the reflections with $l \neq 0$ now occurs at about 170°C, rather than at 130°C, and that the appearance of the CaO reflections is delayed from 205°C to about 307°C.

If the strain relaxation were solely due to thermal annealing, one would not expect such a large increase of the characteristic temperatures between the two runs, the one in vacuum and the other one at 1.78 Torr $P(H_2O)$. On the contrary, with increasing pressure the annealing temperature would be expected to decrease (*17*).

Therefore, the experimental evidence is in favor of a mechanism by which the relaxation of strains or disappearance of defects is controlled by a chemical reaction between the solid hydroxide and the H_2O molecules offered in the gas phase.

Figure 6 shows how the intensity of the reflections 100, 101, 102, 110, and 001 evolves as a function of temperature in the vacuum run performed on the D1B. All reflections except 001 slowly decrease in intensity with increasing temperature up to the point where the first CaO peaks appear. As far as the 001 reflection is concerned, the following behavior can be observed: its intensity seems to decrease more rapidly below 130°C than above this temperature which marks the beginning of the peak sharpening in Figs. 1 and 2 indicated by the straight lines in Fig. 6.

Discussion

Being a layer structure with a perfect cleavage along the basal (001) planes, $Ca(OH)_2$ and its deuterated form $Ca(OD)_2$ cannot sustain any large lattice strains except in its basal (001) planes. This is borne

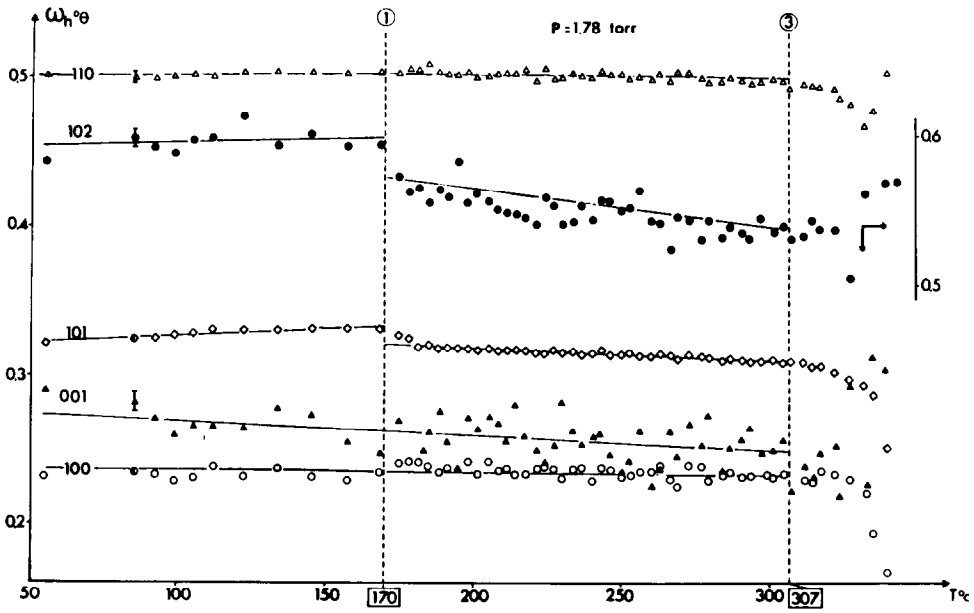

FIG. 4. As Fig. 1, recorded in the presence of a D_2O pressure of 1.78 Torr by neutrons.

out by the Williamson–Hall plot shown in Fig. 3: the *hk*0 reflections provide evidence for minimal distortions in the planes normal to the basal (001) plane, while the 00*l* reflections are indicative of strong distortions within the basal (001) plane.

With increasing temperatures, however, as shown by Figs. 1, 2, 4 and 5, the strains

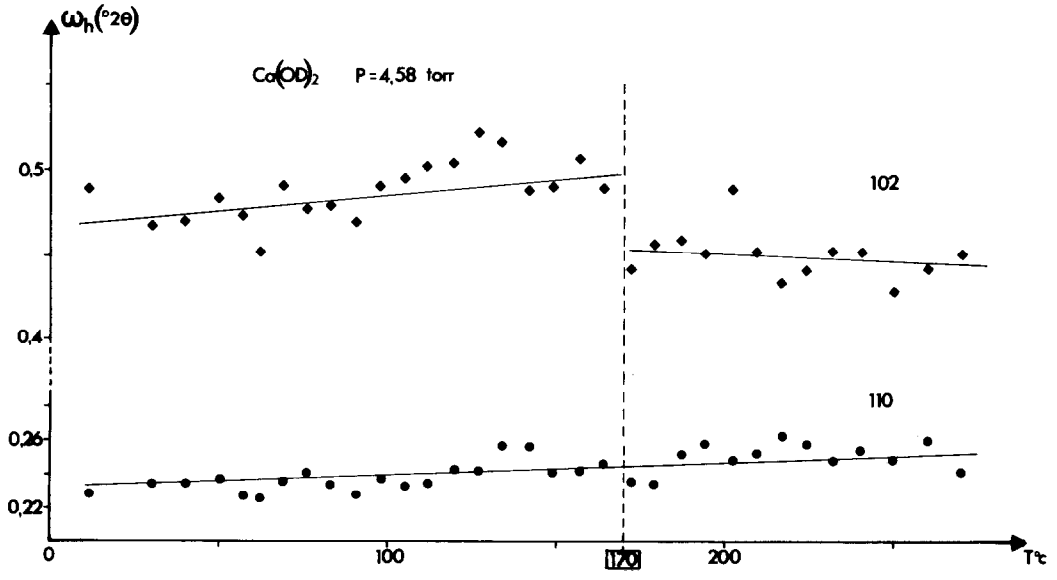

FIG. 5. As Fig. 2, recorded in the presence of a D_2O pressure of 4.58 Torr by x-rays.

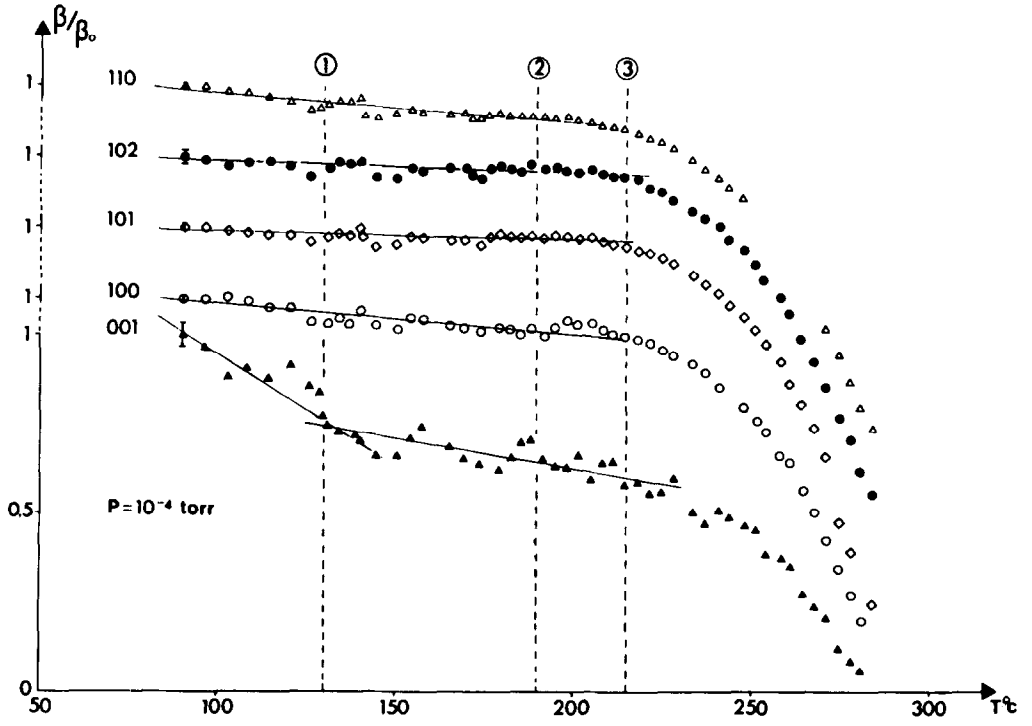

FIG. 6. Temperature dependence of the relative integrated neutron diffraction intensities of $Ca(OD)_2$ in vacuum.

in the (001) plane change abruptly at a given temperature. In the vacuum runs this change occurs at 130°C. It lies well below the onset of D_2O release. Concurrently, as shown by Fig. 6, the temperature dependence of the 001 intensity also changes in a characteristic manner, while that of the other reflections is less affected.

The values of the temperature factors, $B_{hkl} = 8\pi^2 \overline{u^2_{hkl}}$, where u is the displacement of the atoms from their equilibrium positions, are proportional to the absolute temperature and the intensities of the corresponding Bragg reflections must decrease with increasing temperature. On the very short time scale of the scattering event, however, the temperature factor is sensitive not only to contributions from the fast thermal vibrations but also to permanent displacements and to slow fluctuations of the atoms. Hence, strains which offset the atomic positions in a more or less statistical manner will have the same effect as large temperature factors and will manifest themselves in low scattered neutron intensities.

From the intensity versus temperature plots in Fig. 6 it is apparent that the B_{001} value changes quite markedly at 130°C. Since the strain in the (001) plane diminishes concurrently at 130°C (see Figs. 1 and 2), we are led to conclude that the steep slope of the 001 intensity versus temperature curve below 130°C is dominated by strain effects. Conversely, the less steep slope above 130°C should reflect the contributions from the thermal vibrations only. The $00l$ slope is steeper than that of the other lines which reflects the larger mean thermal vibrations in the [001] direction due to the anisotropy of the material. However,

it is to be noted that, even if $l > 1$, the effect is not necessarily more visible because any indices h or $k \neq 0$ counteract the effect.

Additional information about the nature of the lattice disorder causing the strains is available from the runs at slightly elevated D_2O vapor pressure, 1.78 Torr, and from the observed shift of the characteristic temperature from 130 to 170°C (see Figs. 4 and 5). The direction and magnitude of this shift indicate that the gas phase strongly interacts with the solid, probably via a chemisorbed layer of D_2O molecules.

During a study of the dehydration mechanism of $Mg(OH)_2$, $Ca(OH)_2$, and $Al(OH)_3$ it was noted (*6, 7*) that at $T = (T_{\text{decomp.}} - 50)$°C, where $T_{\text{decomp.}}$ stands for the beginning of the actual dehydration, H_2O molecules started to be formed inside the hydroxide matrices. Prior to this event, i.e., at $T < (T_{\text{decomp.}} - 50)$°C, the concentration of mobile protons increased exponentially with increasing temperature without noticeably forming H_2O molecules. Optical data suggest the existence of a proton conduction band approximately 2.0 eV above the valence band in $Mg(OH)_2$. According to these results the mobile protons are in fact delocalized protons thermally activated to this proton conduction band (*8*). Furthermore it was shown that the chemisorption of proton donor and proton acceptor molecules onto the $Mg(OH)_2$, $Ca(OH)_2$, and $Al(OH)_3$ powders strongly modified the proton conductivity behavior.

From these studies it was concluded that the first H_2O molecules are nothing else but delocalized protons trapped on OH^- sites, $OH^- + H^+ \rightleftharpoons H_2O$. These H_2O molecules persist in the sample for some time after cooling. Eventually they decay again, probably by redissociation and recombination of the mobile protons with the deprotonated sites: $H^+ + O^{2-} \rightleftharpoons OH^-$. Upon further heating, as more and more H_2O molecules are formed by the same mechanism, actual dehydration occurs. The dehydration thus

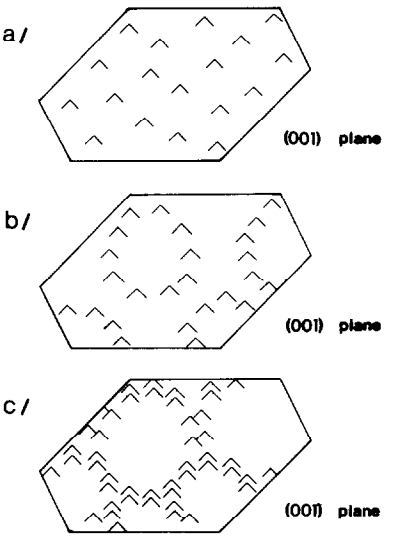

FIG. 7. Schematic representation of a model of the (001) strain distribution associated with protonic defects and compatible with the neutron diffraction data: (a) statistical distribution of H_2O precursors; (b) beginning segregation due to defect clustering, first H_2O formation; (c) interconnecting domain boundaries with high H_2O concentrations.

appears as a sequential step by which H_2O molecules, first formed statistically in the lattice, are released from the surface of the individual hydroxide crystals.

In Fig. 7a the statistical roughness of the (001) planes is modeled schematically. Strain relaxation is expected to occur when the fluctuating defects start to order, forming, maybe, annular or cylindrical domains as suggested by Fig. 7b.

This would be equivalent to the beginning of a spinodal phase segregation: at a critical H_2O concentration the homogeneous phase splits into H_2O-rich and H_2O-poor regions. If the H_2O-rich regions are narrow zones of high strain concentration, corresponding to domain walls, and if the size of the domains is comparable with the coherence length of the neutrons, the (001) temperature factor within these domains will change. Having relaxed the strains the temperature dependence of the 001 intensity will now be domi-

nated by the thermal vibrations only, giving rise to the less steep section at $T > 130°C$ as shown in Fig. 6. At the domain boundaries, where the H_2O concentration is high, no coherent neutron diffraction occurs.

Dehydration, except from the very first atomic layer, is expected to be delayed until the domain boundaries undergo some form of coalescence resulting eventually in an interconnected network which opens fast diffusion pathways for the H_2O molecules to migrate to the outer surface. A possible configuration of this subgrain boundaries is shown schematically in Fig. 7c.

The concept of a spinodal-type phase segregation resulting from an ordering of protonic defects into domain boundaries can explain all observations reported in this paper. It allows for the observed persistence of H_2O in the lattice after cooling, because the redissociation of the H_2O once formed and segregated takes time. It also explains the large effect of a low water vapor pressure in contact with the hydroxide sample. From the earlier studies (*6*) it is known that chemisorbed layers strongly modify the proton conductivity suggesting that the density of delocalized protons and/or deprotonated sites in the solid is affected by the surface layers acting as proton donors or acceptors. Thus, chemisorbed water molecules will modify the temperature at which the critical defect concentration for ordering is reached.

As the present results indicate, the critical temperature and the onset of the actual dehydration are raised by 40 and 90°C, respectively, by 1.78 Torr $P(D_2O)$ implying that, for equal temperatures, the defect concentration is lowered. As long as the type of interaction between the chemisorption layer and the solid hydroxide is unknown, no mechanism can be suggested. It is possible that protons injected from the chemisorbed H_2O layer increase the recombination probability $O^{2-} + H^+ \rightleftharpoons OH^-$, thus lowering the effective concentration of deprotonated sites in the bulk of the hydroxide crystals.

Acknowledgment

We are grateful to the ILL Grenoble for the use of its neutron beam facilities and its technical support.

References

1. G. Bertrand, M. Lallemant, and G. Watelle, *J. Inorg. Nucl. Chem.* **36,** 1303–1309 (1974).
2. G. Bertrand, M. Lallemant, A. Mokhlisse, and G. Watelle, *J. Inorg. Nucl. Chem.* **40,** 819–824 (1978).
3. J. C. Niepce and G. Watelle, *Rev. Int. Hautes Temp. Refract.* **14,** 173–177 (1977).
4. J. C. Niepce, G. Watelle, and N. H. Brett, *J. Chem. Soc. Faraday Trans. 1,* **74,** 1530–1537 (1978).
5. F. Freund and V. Sperling, *Mater. Res. Bull.* **11,** 621–630 (1976).
6. F. Freund and H. Wengeler, *Ber. Bunsenges. Phys. Chem.* **84,** 866–873 (1980).
7. H. Wengeler, R. Martens, and F. Freund, *Ber. Bunsenges. Phys. Chem.* **84,** 873–880 (1980).
8. F. Freund, H. Wengeler, and R. Martens, *J. Chim. Phys.* **77,** 837–841 (1980).
9. W. R. Busing and H. A. Levy, *J. Chem. Phys.* **26,** 563 (1957).
10. N. Gerard and G. Watelle-Marion, *Bull. Soc. Chim. Fr.,* 2631–2635 (1963).
11. N. Gerard, *J. Phys. E.* **5,** 524 (1972).
12. R. Allemand, French patent 73-46051, Dec. 21, 1973.
13. G. K. Williamson and W. H. Hall, *Acta Metall.* **1,** 22 (1953).
14. A. R. Stokes, *Proc. Phys. Soc. London Sect.* **61,** 382 (1948).
15. B. E. Warren and B. L. Averbach, *J. Appl. Phys.* **23,** 497 (1952).
16. O. Pluchery, Thèse de 3 cycle, Université de Dijon (1982).
17. P. Dumas, N. Ea, J. C. Niepce, and G. Watelle, *J. Solid State Chem.* **27,** 317–327 (1979).